J. Fluid Mech. (1993), *vol.* 247, *pp.* 179–204

Oscillatory flow in a stepped channel

By O. R. TUTTY[1] AND T. J. PEDLEY[2]

[1] Department of Aeronautics and Astronautics, University of Southampton, Southampton SO9 5NH, UK

[2] Department of Applied Mathematical Studies, University of Leeds, Leeds LS2 9JT, UK

(Received 27 August 1991 and in revised form 11 June 1992)

Two-dimensional, unsteady flow of a viscous, incompressible fluid in a stepped channel has been studied by the numerical solution of the Navier–Stokes equation using an accurate finite-difference method.

With a sinusoidal mass flow rate, the problem has three governing parameters: the Reynolds number, the Strouhal number, and the step height. The effects on the flow of varying all three parameters has been investigated systematically. In appropriate parameter regimes, a strong 'vortex wave' is generated during the forward phase when the flow is over the step into the expansion. Secondary effects on the wave can result in a complex flow pattern with each major structure of the flow consisting of an eddy with more than one core. No such wave is found during the reverse phase of the flow. The generation and development of the wave is examined in some detail, and our results are compared and contrasted with those of previous studies, both experimental and theoretical, of flow in non-uniform vessels.

1. Introduction

Recently there has been considerable interest in unsteady flow in non-uniform channels (e.g. Cherdron, Durst & Whitelaw 1978; Armaly *et al.* 1983; Sobey 1985; Pedley & Stephanoff 1985; Ralph & Pedley 1988, 1989, 1990; Tutty 1992), a problem which is important in both engineering and biomechanics, and which is of intrinsic interest because of the richness and complexity of the flow patterns that can occur in a two-dimensional flow even in a relatively simple geometry.

In most of the studies referred to above, a train of propagating waves was observed to grow downstream of the non-uniformity in the channel wall(s), with regions of closed streamlines ('eddies') beneath the crests and above the troughs. We shall call these 'vortex waves' in all cases, even though the mechanism of their generation may be different in different examples. Sobey (1985) performed a set of experiments and a limited number of computations on both steady and unsteady flow through rigid channels with both symmetric and asymmetric expansions. Waves were found in both cases, but Sobey felt that the wave in the symmetric channel was fundamentally different from that in the asymmetric channel, the former being the result of a shear-layer instability, while the latter was a vortex wave forced by the asymmetry of the channel. It is the asymmetric problem with the forced vortex wave which is investigated here.

Pedley & Stephanoff (1985) and Ralph & Pedley (1988, 1989, 1990) have performed a series of experiments and calculations for flow in a channel with an indentation moving in and out on one wall, the flow being steady when the indentation was stationary. They found a vortex wave for both viscous and inviscid flow, but there were significant differences between the two cases. A much more

complex flow pattern was obtained in the viscous case, including 'eddy doubling' in which an eddy which initially shows a high degree of longitudinal symmetry becomes markedly asymmetric and eventually splits into at least two separate corotating eddies. Pedley & Stephanoff (1985) developed a weakly nonlinear inviscid theory for the flow in a channel where there is a forced, time-dependent disturbance to the flow. This theory was used successfully to explain and interpret the experimental observations in the moving-wall problem for a certain range of parameter values. In particular the appearance and propagation of the waves were predicted with quantitative accuracy, although details of the eddies were not included. In this theory, the mechanism for generation of the waves is associated with the displacement of the vorticity gradient in the oncoming Poiseuille flow, not with viscous disturbances at the channel walls, which led Pedley & Stephanoff to call the wave a 'vorticity wave'.

In this paper we present numerical solutions of the Navier–Stokes equations for oscillatory flow in a rigid channel with a sudden expansion in the form of a step. A sinusoidally varying mass flow rate is assumed, and we investigate in turn the effects of varying the three governing parameters: the Reynolds number, the Strouhal number (the unsteadiness parameter), and the step height. It would in addition be possible to vary the form of the channel expansion and of the mass flow rate, but these aspects are not addressed. We note, however, that Sobey (1985) performed experiments with oscillatory flow in a channel with a 45° expansion as well as a 90° step, and Tutty (1992) gives numerical solutions for non-sinusoidal pulsatile flow in a constricted channel; the results of these studies suggest that the vortex wave phenomenon is robust to such changes.

The success of the weakly nonlinear inviscid theory in predicting the generation and propagation of the vortex wave in the case of a moving indentation with a steady upstream flow (Pedley & Stephanoff 1985) suggested that we should look for a corresponding theory in the case of oscillatory flow past a fixed indentation. Such a theory has been developed (Tutty & Pedley 1992), and testing it formed part of the motivation for the present study. In this case there is qualitative agreement with some of the results, such as the predictions that waves will be generated and that those closest to the step remain approximately stationary, without propagating. However, the predicted dependence of the wavelength on the governing parameters (e.g. decreasing as the step size increases) is not borne out by the Navier–Stokes solutions and the theory cannot be regarded as successful.

An important motivation for the present and much of the earlier work is physiological in nature, because of a hypothesis linking regions of low or oscillating wall shear stress in arteries to a local predisposition to develop atherosclerosis (see Ku *et al.* 1985*a*, *b*). Many of the sites that are prone to atherosclerosis occur where there is a rapid change in the cross-sectional area or shape of the vessels, so that flow separation is to be expected. The effect of the vessel geometry on the wall shear stress (or wall vorticity) distribution is therefore of considerable interest. Predicted values of the wall vorticity are presented below.

The formulation of the problem is given in §2, and the numerical method in §3, including a discussion of computational accuracy. The basic results are presented in §4, and the generation and development of the vortex wave are discussed in detail in §5, with some concluding remarks in §6.

2. Formulation

The channel expansion takes the form of a step at $x^* = 0$ from a dimensional width of a^* to $(1+\epsilon)a^*$, with the lower wall undisturbed (figure 1). The coordinates are non-dimensionalized on the upstream channel width so that $(x^*, y^*) = a^*(x, y)$. The corresponding velocity components are $U_0^*(u, v)$ where the reference velocity is $U_0^* = Q_0^*/a^*$ and Q_0^* is the peak volumetrie flow rate. The dimensional time is given by T^*t where T^* is the period of oscillation of the flow.

The Reynolds number Re and the Strouhal number St are defined by

$$Re = U_0^* a^*/\nu, \quad St = a^*/(U_0^* T^*), \tag{2.1}$$

where ν is the kinematic viscosity. The vorticity transport equation becomes

$$St\frac{\partial \zeta}{\partial t} + u\frac{\partial \zeta}{\partial x} + v\frac{\partial \zeta}{\partial y} = \frac{1}{Re}\nabla^2 \zeta, \tag{2.2}$$

where the vorticity ζ is given in terms of the streamfunction ψ by

$$\zeta = -\nabla^2 \psi. \tag{2.3}$$

As usual,

$$(u, v) = \left(\frac{\partial \psi}{\partial y}, -\frac{\partial \psi}{\partial x}\right). \tag{2.4}$$

Note that the above non-dimensionalization differs from that of Sobey (1985) in that it is based on the channel width rather than half the width. Thus, for a particular flow, the values of the Reynolds and Strouhal numbers are double those of Sobey.

The boundary conditions are: no-slip at the walls,

$$u = v = 0 \quad \text{on} \quad y = 0 \quad \text{and} \quad y = y_w, \tag{2.5}$$

where

$$y_w = \begin{cases} 1, & x < 0 \\ 1 < y < 1+\epsilon, & x = 0 \\ 1+\epsilon, & x > 0 \end{cases} \tag{2.6}$$

gives the position of the upper wall; parallel flow upstream and downstream, i.e.

$$\frac{\partial^n \psi}{\partial x^n} \to 0, \quad \frac{\partial^n \zeta}{\partial x^n} \to 0 \quad \text{as} \quad x \to \pm\infty, \tag{2.7}$$

where $n \geqslant 1$ (see below); and a sinusoidal flow rate

$$\left.\begin{aligned} \psi &= 0 && \text{on } y = 0, \\ \psi &= \psi_w = \sin(\pi t) && \text{on } y = y_w. \end{aligned}\right\} \tag{2.8}$$

Thus we have a net flow from left to right during the first half of the flow cycle ($i < t < i+\frac{1}{2}$ where i is an integer) and from right to left during the second half ($i+\frac{1}{2} < t < i+1$). The initial condition is that of no motion:

$$\psi = \zeta = 0 \quad \text{as} \quad t = 0. \tag{2.9}$$

The problem defined here has three governing parameters: Re, St, and ϵ, the magnitude of the channel expansion. The results presented below are based on

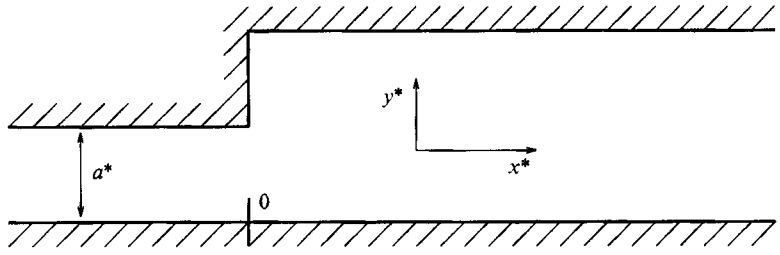

FIGURE 1. Channel geometry (physical).

varying the parameters around those for a reference case which has $Re = 500$, $St = 0.006$, and $\epsilon = 1$. This set of parameters produces an interesting flow pattern and is broadly consistent with those used by Sobey in his experimental work.

3. Numerical methods

3.1. *Computational formulation and grid*

Rather than placing a computational grid on the physical domain, we have adopted a more flexible approach. A conformal transformation was used to map the physical channel on a straight channel of unit width (figure 2), and the transformed version of the governing equations was solved in computational space. The Navier–Stokes equations maintain their form under a conformal transformation, and this approach has the advantage that a range of problems can be solved by supplying the Jacobian of the appropriate transformation to a general Navier–Stokes solver, and mapping the results back to physical space when the calculation is complete.

Suppose the reverse mapping from computational to physical space is given by

$$z = W(Z), \tag{3.1}$$

where $z = x+\mathrm{i}y$, $Z = X+\mathrm{i}Y$, and W is a complex function. The vorticity transport equation and the Poisson equation (2.2), and (2.3) become

$$J St\frac{\partial\zeta}{\partial t}+U\frac{\partial\zeta}{\partial X}+V\frac{\partial\zeta}{\partial Y}=\frac{1}{Re}\nabla^2\zeta \tag{3.2}$$

and

$$J\zeta = -\nabla^2\psi \tag{3.3}$$

respectively, where $J = \partial(x,y)/\partial(X,Y)$, ∇^2 is now the Laplacian in computational space, and

$$(U,V) = \left(\frac{\partial\psi}{\partial Y}, -\frac{\partial\psi}{\partial X}\right). \tag{3.4}$$

This is the system of equations solved in the present study.

The mapping is essentially a two-step process: an exponential transform which maps the uniform channel in Z-space to a half-plane, followed by a Schwarz–Christoffel transform which maps the half-plane to the degenerate polygon formed by the physical channel. Combining these steps produces

$$\mathrm{d}z/\mathrm{d}Z = (1-\mathrm{e}^{\pi(Z-a)})^{\frac{1}{2}}(1-\mathrm{e}^{\pi(Z-b)})^{-\frac{1}{2}}, \tag{3.5}$$

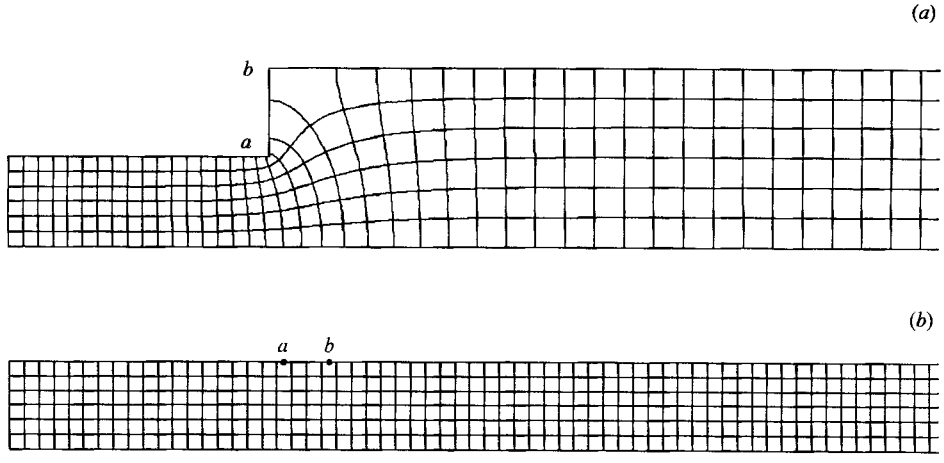

FIGURE 2. The mapping from physical (*a*) to computational space (*b*) and a sample (crude) computational mesh.

where the corners $(x, y) = (0, 1)$ and $(0, 1+\epsilon)$ in physical space map to $Z = a$ and b respectively in the computational space, with $\mathrm{Im}\,(a) = \mathrm{Im}\,(b) = 1$, and

$$b - a = (2/\pi)\ln(1+\epsilon), \tag{3.6}$$

which ensures that the magnitude of the channel expansion is correct. Given a and b, the Jacobian J is calculated directly from (3.5) since $J = |\mathrm{d}z/\mathrm{d}Z|^2$.

The integration of (3.5) to obtain (the real parts of) a and b and the mapping between the grids must be performed numerically. The only difficulty arises from the singularity at $Z = b$ which, if not handled carefully, could adversely affect the accuracy of the calculation. The integration procedure is based on that of Sridhar & Davis (1985). In moving from Z_0 and Z_1 in computational space the corresponding change in physical space is given by

$$z_1 - z_0 = \left[\frac{1-\mathrm{e}^{\pi(\bar{Z}-a)}}{\bar{Z}-a}\right]^{\frac{1}{2}}\left[\frac{(Z-a)^{\frac{3}{2}}}{\frac{3}{2}}\right]_{Z_0}^{Z_1}\left[\frac{1-\mathrm{e}^{\pi(\bar{Z}-b)}}{\bar{Z}-b}\right]^{-\frac{1}{2}}\left[\frac{(Z-b)^{\frac{1}{2}}}{\frac{1}{2}}\right]_{Z_0}^{Z_1}, \tag{3.7}$$

where $\bar{Z} = \frac{1}{2}(Z_0 + Z_1)$.

The computational grid used was a uniform rectangular grid in (X, Y). Details are given below. A sample (crude) grid is shown in figure 2. The clustering of the points near the convex corner is a useful feature as relatively large errors are expected to arise there from the singularity in the vorticity. The comparatively large spacing of the grid near the concave corner (exaggerated in figure 2 by the crudity of the sample grid) caused no problems as the flow is not particularly vigorous there. The grid lines with constant X and Y are respectively the streamlines and equipotential lines for the idealized case of inviscid irrotational flow.

3.2. *Finite difference scheme*

We use a Crank–Nicolson scheme which is second-order accurate in time and fourth-order in space. The scheme is essentially an unsteady version of that of Dennis & Hudson (1989), but it was obtained in a different manner by directly applying Numerov's method in which the differential equations are used to express higher-

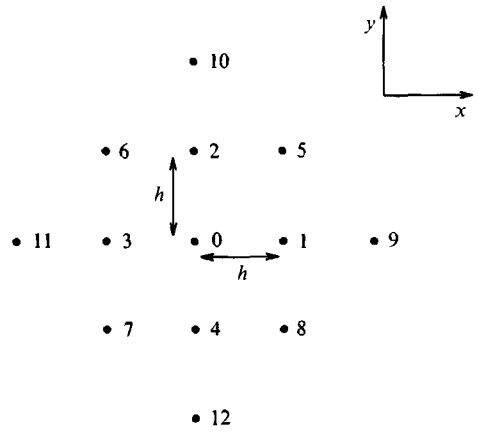

FIGURE 3. Labelling of grid points.

order derivatives in terms suitable for approximation in compact form. Labelling the grid points as in figure 3, we obtain

$$\frac{\psi_1+\psi_2+\psi_3+\psi_4-4\psi_0}{h^2}-(\nabla^2\psi)_0=\frac{h^2}{12}\left(\frac{\partial^4\psi}{\partial X^4}+\frac{\partial^4\psi}{\partial Y^4}\right)_0+O(h^4), \tag{3.8}$$

where h is the grid step. From (3.3)

$$\nabla^4\psi=-\nabla^2(J\zeta)_0.$$

Therefore

$$\frac{\psi_1+\psi_2+\psi_3+\psi_4-4\psi_0}{h^2}+(J\zeta)_0=-\frac{h^2}{12}\left(2\frac{\partial^4\psi}{\partial X^2\partial Y^2}+\nabla^2(J\zeta)\right)_0+O(h^4). \tag{3.9}$$

Substituting standard second-order finite difference formulae into the right-hand side of (3.9) gives a fourth-order correction to the standard second-order scheme formed by setting the left-hand side to zero. This produces

$$\begin{aligned}4(\psi_1+\psi_2+\psi_3+\psi_4)+\psi_5+\psi_6+\psi_7+\psi_8-20\psi_0\\ =-\tfrac{1}{12}h^2((J\zeta)_1+(J\zeta)_2+(J\zeta)_3+(J\zeta)_4+8(J\zeta)_0),\end{aligned} \tag{3.10}$$

a fourth-order finite difference equation which is compact in that it uses only the nine points closest to the centre and thus can be applied directly at points adjacent to the boundary, unlike the usual fourth-order scheme.

Applying the same method to the vorticity transport equation (3.2) gives

$$\begin{aligned}&\frac{\zeta_1+\zeta_2+\zeta_3+\zeta_4-4\zeta_0}{h^2}-\hat{U}_0\frac{\zeta_1-\zeta_3}{2h}-\hat{V}_0\frac{\zeta_2-\zeta_4}{2h}-H_0\\ &=\frac{h^2}{12}\Big\{-2\frac{\partial^4\zeta}{\partial X^2\partial Y^2}+(\nabla^2\hat{U}-\hat{\boldsymbol{U}}\cdot\boldsymbol{\nabla}\hat{U})\frac{\partial\zeta}{\partial X}+(\nabla^2\hat{V}-\hat{\boldsymbol{U}}\cdot\boldsymbol{\nabla}\hat{V})\frac{\partial\zeta}{\partial Y}\\ &\quad+\left(2\frac{\partial\hat{U}}{\partial X}-\hat{U}^2\right)\frac{\partial^2\zeta}{\partial X^2}+\left(2\frac{\partial\hat{V}}{\partial Y}-\hat{V}^2\right)\frac{\partial^2\zeta}{\partial Y^2}+2\left(\frac{\partial\hat{U}}{\partial Y}+\frac{\partial\hat{V}}{\partial X}-\hat{U}\hat{V}\right)\frac{\partial^2\zeta}{\partial X\partial Y}\\ &\quad+2\hat{U}\frac{\partial^2\zeta}{\partial X\partial Y^2}+2\hat{V}\frac{\partial^2\zeta}{\partial X^2\partial Y}+\nabla^2H-\hat{\boldsymbol{U}}\cdot\boldsymbol{\nabla}H\Big\}_0+O(h^4),\end{aligned} \tag{3.11}$$

where $(\hat{U}, \hat{V}) = Re(U, V)$ and $H = ReStJ\,\partial\zeta/\partial t$. The left-hand side of this equation is the standard second-order difference scheme while the $O(h^2)$ term on the right provides a fourth-order correction when standard second-order finite difference formulae are substituted (strictly the truncation error of (3.11) is $O(Re^2h^4)$, which gives an error of $O(Re\,h^4)$ when the equation is divided by Re to return it to standard form).

Compact fourth-order formulae which use values of the vorticity as well as the streamfunction can be derived for the transformed 'velocity' (U, V). However, these formulae are likely to have large errors near the convex corner where the vorticity is singular, and the more straightforward five-point formulae were used when possible. That is, we use

$$\left.\begin{aligned} U_0 &= \left(\frac{\partial\psi}{\partial Y}\right)_0 = \frac{8(\psi_2-\psi_4)-\psi_{10}+\psi_{12}}{12h} \\ V_0 &= -\left(\frac{\partial\psi}{\partial X}\right)_0 = -\frac{8(\psi_1-\psi_3)-\psi_9+\psi_{11}}{12h} \end{aligned}\right\} \tag{3.12}$$

at points away from the boundary. At points adjacent to the boundary at least one of these formulae will not be applicable as it involves a point outside the grid for which ψ is undefined. At such points the boundary condition for the velocity can be incorporated to produce an alternative fourth-order formula. For example, if the velocity is zero at point 4, then $U_4 = 0$, and we obtain

$$U_0 = \frac{9\psi_0+9\psi_2-17\psi_4-\psi_{10}}{18h} \tag{3.13}$$

which has truncation error $O(h^4)$. Strictly, with the velocity calculated from (3.12) and (3.13), the vorticity transport equation is not compact. However, it still has the advantage that, given the velocity, it can be applied directly at all interior points of the grid.

A Crank–Nicolson scheme is obtained by substituting

$$\left(\frac{\partial\zeta}{\partial t}\right)^{n+\frac{1}{2}} = \frac{\zeta^{n+1}-\zeta^n}{\Delta t} \tag{3.14}$$

at all points, and replacing the ζ by

$$\zeta^{n+\frac{1}{2}} = \tfrac{1}{2}(\zeta^{n+1}+\zeta^n), \tag{3.15}$$

with similar formulae for $\hat{U}$ and $\hat{V}$, where ζ^n is the estimate of ζ at time $t_n = n\Delta t$. This produces an implicit finite difference equation which is second-order accurate in time.

It remains to specify the numerical boundary conditions. Upstream ($x \to \mp\infty$ according to whether the flow is from the left or the right) parallel flow was assumed and ψ and ζ were calculated from the numerical scheme by eliminating all x-derivatives. Downstream, a conventional derivative condition was imposed, namely

$$\frac{\partial^2\psi}{\partial X^2} = \frac{\partial^2\zeta}{\partial X^2} = 0. \tag{3.16}$$

In effect this assumes parallel flow downstream, but avoids the problems caused by the small reflected disturbances which can arise if values of ψ and ζ are fixed at a boundary at which there is an outward flow.

On the walls the streamfunction was specified by (2.7), while the vorticity was calculated by a finite difference form of

$$\zeta = -\frac{1}{J}\frac{\partial^2 \psi}{\partial Y^2}. \tag{3.17}$$

With a second-order streamfunction–vorticity scheme, the compact Woods (1954) formula is commonly used (e.g. Ralph & Pedley 1988). Alternatively, a one-sided difference formula could be used. Previous work (unpublished) with the present fourth-order scheme applied to the steady driven cavity problem showed that, provided the grid was sufficiently refined, the results obtained when using a one-sided difference formula were not significantly different from those obtained with the compact formula analogous to that of Woods. However, for the driven cavity problem, convergence of the iterative scheme was faster with the one-sided formula. Hence a similar formula was used here. For example, if point 12 is on the lower wall, we use

$$\zeta_{12} = \frac{-415\psi_{12} + 576\psi_4 - 216\psi_0 + 64\psi_2 - 9\psi_{10}}{7h^2 J_{12}}, \tag{3.18}$$

where the zero normal velocity condition was used in deriving this equation. A similar equation was used on the upper wall.

3.3. *Solution procedure*

An iterative line relaxation scheme was used to solve the system of nonlinear finite difference equations given above. For the streamfunction equation (3.10), a tridiagonal system was formed by taking the equations along a grid line with constant Y (or X), and treating the values of ψ on that line as unknowns and the other values of ψ and ζ as known using current estimates. A similar tridiagonal system can be defined using the vorticity equation (3.11). However, instead of using the finite difference equation as written in (3.11), with the left-hand side of the equation forming the iteration matrix, part of the fourth-order term on the right was moved to the left, in the manner of Dennis & Hudson (1989), to increase the diagonal dominance of the iteration matrix, and thus improve the stability of the iteration procedure. The remaining part of the fourth-order term was treated as a forcing term and was updated every complete iteration.

The basic solution procedure for each time step was to sweep through the grid for the streamfunction equation (3.10) updating all values of ψ, evaluate the new values of the 'velocity' (U, V) from (3.12) and (3.13), update the boundary vorticity and the forcing terms for the vorticity equation, then sweep through the grid finding the new estimates for the vorticity. The procedure was repeated until convergence was achieved. Latest values were used where possible and thus the iteration scheme is line Gauss–Seidel in nature. A sweep through the grid may be carried using lines along the X-direction (constant Y), along Y (constant X), or alternating the two as in an ADI method. All three were tried and, perhaps surprisingly, there was little difference in the computing time required for each. Taking lines in the X-direction was used as it was marginally fastest in the test case.

With a scalar computer, this iteration scheme can be implemented in the obvious manner, solving each matrix equation in turn. However, this would be very inefficient for a vector machine because of the data dependency in the matrix solution algorithm. Thus the basic procedure was modified by introducing red-black

ordering and a block solution method. That is, a set of independent tridiagonal matrix equations was formed by taking every second line in X, and these were solved simultaneously rather than consecutively by making the innermost loop a sweep across the matrices. A second block solution updated the rest of the values. This block solution method enabled the code to vectorize while retaining superior stability and convergence properties over, say, the simpler Jacobi method which would also vectorize. On a single Cray XMP processor the code ran at 115 to 130 Mflops, depending on the vector length.

The convergence criterion was that for all the grid points

$$\max |\psi^{(m+1)} - \psi^{(m)}| < \text{tol}, \tag{3.19}$$

where m indicates the iteration count. The standard value of tol was 10^{-7}.

At each time step the initial guess was obtained by a third-order extrapolation in time from previous values.

3.4. *Accuracy*

A number of factors will affect the accuracy of the numerical solution: the positions of the upstream and downstream boundaries, the (spatial) grid step, the time step, and the tolerance (tol) of the iterative procedure.

Test runs were performed with flow over the step and the upstream (left) boundary at a distance of approximately 5, 10, and 15 units (in the computational space) from the step. The difference between the solutions for 5 and 10 was small, and negligible for 10 and 15. The results presented below have the upstream boundary at $X \approx 10$, with the exception of those in figures 5 and 6, when the roles of the left- and right-hand boundaries reverse with the bulk flow. At $t = 0.5$ the right-hand boundary was fixed in position and then treated as an upstream boundary, with the left-hand boundary taking the downstream role. The roles of the left and right boundaries were swapped similarly at $t = 1.0$ when the flow changes direction for the second time.

Throughout the calculations, a check was kept on the change in the streamfunction at a distance of one channel width (in computational space) upstream of the downstream boundary. If the change in ψ between successive grid points (i.e. $|\psi^n_{i+1,j} - \psi^n_{i,j}|$) became greater than 10tol the computational domain was expanded downstream.

Extensive investigations were made of the effect on the solution of the grid step h. The method is of fourth spatial order, and was found to behave accordingly, except close to the convex corner where, as expected, the singularity in the vorticity degraded the performance. Also as expected, the grid resolution required varied with the parameters of the flow; more grid points were needed to obtain a fully converged solution with a more vigorous flow. Vorticity gradients are highest near the walls, and the most sensitive indicator of error in the solution was found to be the vorticity on the walls. Figure 4(*a*) shows the lower-wall vorticity at $t = 0.45$ for the case with $Re = 500$, $St = 0.006$, and $\epsilon = 2$, for $h = \frac{1}{32}, \frac{1}{48}, \frac{1}{64}$, and $\frac{1}{80}$. In terms of convergence with the grid step, this particular example has the worst behaviour of all the parameter sets for which results are presented. A more typical example is shown in figure 4(*b*), which gives the variation in wall vorticity with h for $Re = 750$, $St = 0.006$, and $\epsilon = 1$ at $t = 0.45$. Similar behaviour was found for the vorticity on the upper wall, with, in particular, the vorticity near the convex corner approaching a limit as the grid is reduced in size. Most of the results presented below are for $h = \frac{1}{64}$, although $h = \frac{1}{48}$ was used for some of the problems with a less vigorous flow (e.g. $Re = 250$, $St = 0.006$, and $\epsilon = 1$).

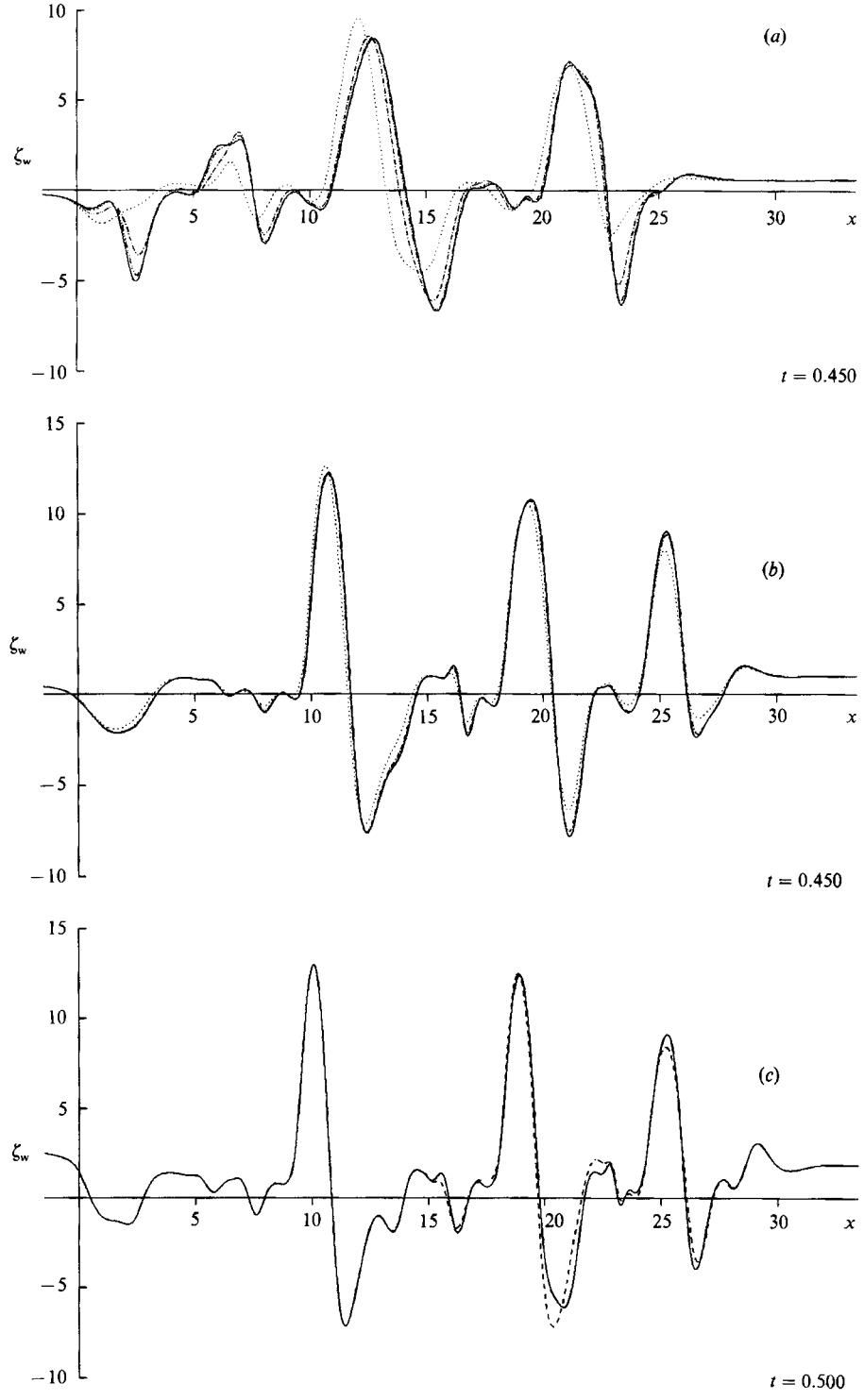

FIGURE 4. The effect of the mesh size and tolerance on the lower-wall vorticity. (*a*) $Re = 500$, $St = 0.006$, $\epsilon = 2$, $t = 0.45$: ....., $h = 1/32$; —·—·—, $h = 1/48$; —··—, $h = 1/64$; ——, $h = 1/80$. (*b*) $Re = 750$, $St = 0.006$, $\epsilon = 1$, $t = 0.45$: ....., $h = 1/32$; —·—·—, $h = 1/48$; ——, $h = 1/64$. (*c*) $Re = 750$, $St = 0.006$, $\epsilon = 1$, $t = 0.5$, $h = 1/64$; – – –, tol $= 10^{-6}$; ——, tol $= 10^{-7}$.

Note that no specific provision was made for the singularity at the convex corner (a on figure 2): instead the position of the left-hand boundary was adjusted so that the corner always lay halfway between grid points. The concave corner (b) caused no problems as the vorticity is zero there.

To obtain a fully converged solution it is vital that the tolerance on the iterative procedure be set small enough. The tolerance required depended on the flow parameters and the grid, a smaller value in general being needed for a more vigorous flow and/or a smaller value of h. Figure 4(c) shows the lower-wall vorticity at $t = 0.5$ for $Re = 750$, $St = 0.006$, and $\epsilon = 1$ with tol $= 10^{-6}$ and 10^{-7}. For this case, refining the grid with tol $= 10^{-6}$ led to an erratic variation around the converged solution which was obtained with tol $= 10^{-7}$ (see figure 4b), rather than to the converged solution. All the results presented below have tol $= 10^{-7}$.

The solutions obtained were relatively insensitive to the time step used, presumably because of the fully implicit nature of the numerical scheme. Test runs showed little difference between solutions with $\Delta t = 0.005$, 0.0025, and 0.001 25. The results presented below usually have $\Delta t = 0.0025$, although values with the smaller time step (0.001 25) were used when available. The computational time required was not strongly dependent on the time step, as the number of iterations required per time step decreased with Δt. However, for any particular combination of flow parameters and grid, the size of the minimum time step was limited by the convergence properties of the iterative procedure.

4. Results

The feature of greatest interest is the large-amplitude vortex wave which develops during the forward part of the flow when the fluid is travelling over the step into the expanded portion of the channel (see e.g. figure 5). The growth and development of this wave are discussed in detail in §5 below. *A priori*, it might be expected that the wavefront is convected with the flow, and this concept provides a useful framework in which to examine the effect on the wave of varying the parameters. The non-dimensional equations for the motion of a particle in the flow are

$$\frac{\mathrm{d}}{\mathrm{d}t}(x, y) = \frac{1}{St}(u, v), \tag{4.1}$$

so if the wave front is convected with the flow, the dimensionless distance the wave travels downstream should show a strong dependence on St but a relatively weak dependence on Re, since Re occurs only in the equations, not the boundary conditions or (4.1). Our results show that, for any particular channel (i.e. for a given ϵ), this hypothesis is reasonable, as long as the wave is sufficiently strong. However, qualitative agreement between the extent of the wave and the distance travelled by a particle in parallel flow is poor for step heights other than $\epsilon = 1$ (§4.4). Another general prediction is that if the principal features of the flow show only a weak dependence on Re then inviscid mechanisms are likely to be dominant.

In §4.1 the results are presented for the reference case with a channel that doubles in width at $x = 0$ ($\epsilon = 1$), and we then consider in turn the effects of varying Re, St and e.

4.1. $Re = 500$, $St = 0.006$, $e = 1$

Calculations were performed for this problem to $t = 1.5$, with streamlines to $t = 1.2$ shown in figure 5: the starting transients have essentially died out by $t = 0.2$, and the sequence from $t = 0.2$ to 1.2 is periodic (in fact there is little difference between the

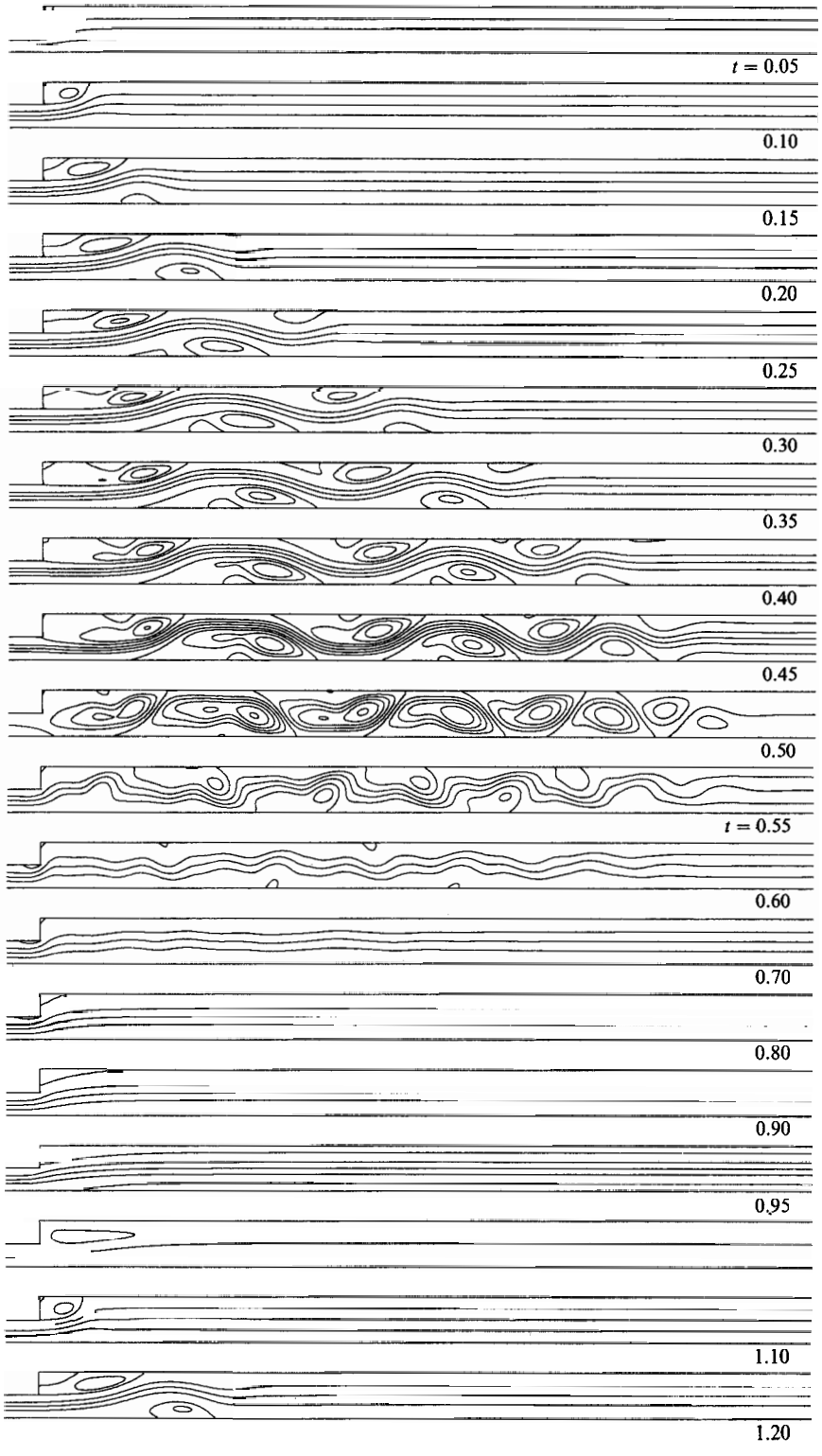

FIGURE 5. Streamlines $Re = 500$, $St = 0.006$, $\epsilon = 1$, $-1.5 \leqslant x \leqslant 33.5$. The values plotted are in increments of 0.05 above ψ_w and below zero, and in increments of $\frac{1}{4}\psi_w$ between zero and ψ_w. Unless specifically mentioned, the same values are used for the other streamfunction plots.

Re =	250		500		750	
t	l	u	l	u	l	u
0.05	0.000	0.004	0.000	0.008	0.000	0.011
0.10	0.000	0.050	0.000	0.073	0.000	0.084
0.15	−0.001	0.066	−0.010	0.087	−0.018	0.100
0.20	−0.011	0.077	−0.057	0.095	−0.090	0.104
0.25	−0.022	0.084	−0.077	0.106	−0.110	0.112
0.30	−0.033	0.089	−0.092	0.117	−0.126	0.122
0.35	−0.045	0.090	−0.114	0.125	−0.147	0.141
0.40	−0.064	0.095	−0.143	0.135	−0.176	0.179
0.45	−0.099	0.110	−0.186	0.182	−0.220	0.229
0.50	−0.171	0.156	−0.255	0.258	−0.302	0.299

TABLE 1. Variation of maximum eddy strengths with the Reynolds number: l gives the minimum value of the streamfunction (which is zero on the lower wall) and u the difference between the maximum value of the streamfunction and the value on the upper wall. $St = 0.006$, $e = 1$.

streamlines at $t = 0.15$ and those at $t = 1.15$). Although St is small this flow is far from quasi-steady, with a strong vortex wave which propagates well down the channel. The distance travelled by a fluid particle along the centre of a channel of width 2 was calculated, assuming parallel flow in the channel. Starting from rest, a particle at $x = 0$ at $t = 0$ would be at $x = 16.1$ at $t = 0.25$ when the mass flow is at its peak, and at $x = 36.5$ at $t = 0.5$ when there is no net flow. The particle would return during the reverse flow phase, reaching $x = 3.21$ at $t = 1$ (not $x = 0$ because of the starting transients), and then move to $x = 16.8$ at $t = 1.25$ and $x = 36.6$ at $t = 1.5$, etc. The downstream motion of the wave shown in figure 5 is broadly consistent with these values, both in the total length of the wave and in that the wave front propagates further during the deceleration of the forward flow ($t = 0.25$ to 0.5) than during the acceleration ($t = 0$ to 0.25). Also, the full numerical solution was examined at $t = 0.25$ and the crest of the wave furthest downstream was located. A particle located at the centre of the channel on this crest was then tracked downstream until $t = 0.5$, and indeed appeared to travel with the wave front.

It can be seen from figure 5 that, although eddies develop beneath the waves in the first quarter of the cycle, they become much stronger during the second quarter when the mean flow is decelerating. This can also be seen from table 1 which gives the maximum eddy strengths for this problem. As well as increasing in strength, the eddies increase in size with the result that the movement of the core streamlines away from the centreline becomes increasingly pronounced until at $t = 0.5$ the eddies span the channel. Upstream of the larger eddies a second, smaller, eddy develops as the main flow moves away from the wall. This secondary eddy grows until it joins the main eddy (e.g. at $t = 0.275$ for the first eddy on the lower wall), which then has two corotating cores and a smaller counter-rotating eddy trapped between the main eddy and the wall. The eddy trapped on the wall is very weak and decreases in size as t approaches 0.5, while the secondary corotating core of the main eddy grows in strength. This secondary disturbance will be discussed in further detail below (§5).

The decelerated flow reverses first at the walls, so that at $t = 0.5$ (when the mean flow reverses) the flow both far upstream and far downstream is reversed near the walls and forward in the centre of the channel. However, by $t = 0.530$ the flow in the centre has reversed both upstream and downstream. During the early part of the reversed flow, the eddies, which are now attached to the wall opposite the one on

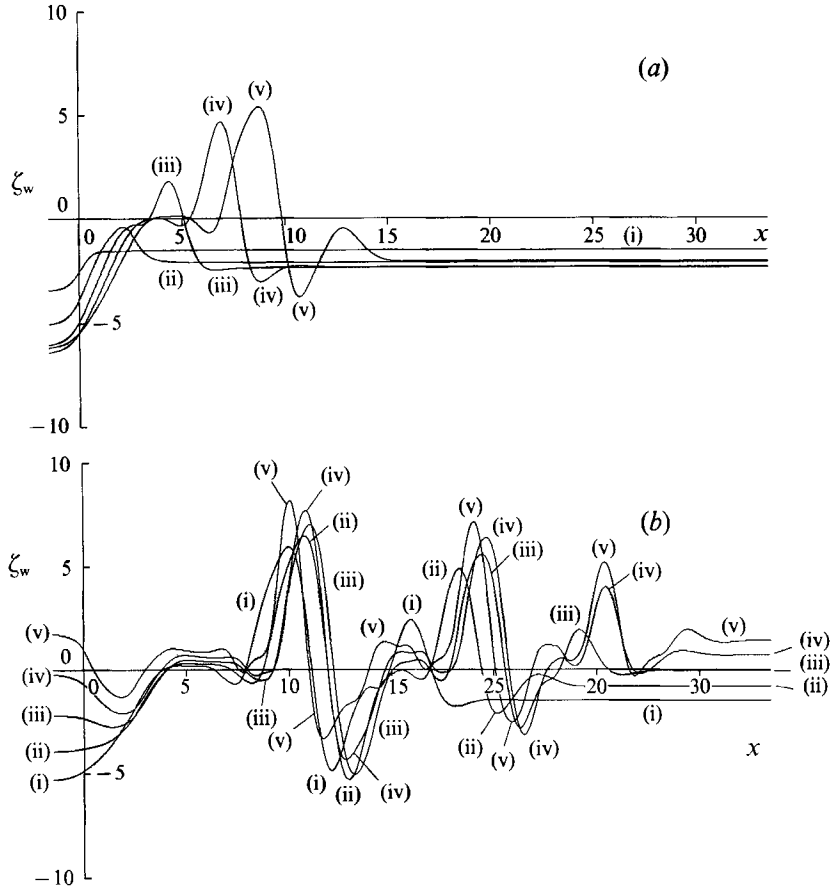

FIGURE 6(*a*, *b*). For caption see facing page.

which they originated, rapidly lose their strength, although some waviness can be found in the flow in the expanded portion of the channel up to $t = 0.75$ when the reversed flow rate is at its peak. By this stage an eddy has formed in the step with another very small eddy in the narrow part of the channel at the corner. As the reverse flow decelerates, the eddy in the step expands, while that on the top disappears. During the reversed flow phase, a small disturbance is carried a considerable distance up the channel past the constriction, slowly matching to parallel flow, but no evidence was found for a large-amplitude wave. In this case, wave generation occurs only when the flow is directed into the wider part of the channel, although the unsteadiness and complexity of the flow makes it impossible to attribute this directly to the accompanying flow deceleration.

When they are first formed the individual eddies show some downstream motion, but the wave can be described in general terms as a standing wave with a positive group velocity but little or no phase velocity (see Tutty & Pedley 1992). Figure 5 shows clearly that the wavelength decreases along the channel. Wave crest and trough positions were obtained from the turning points of the centre streamline (see figure 8 below), and the (primary) wavelength was estimated from these values. Near $t = 0.5$ the wavelength was found to vary from approximately 11 near the step to approximately 4 near the wavefront.

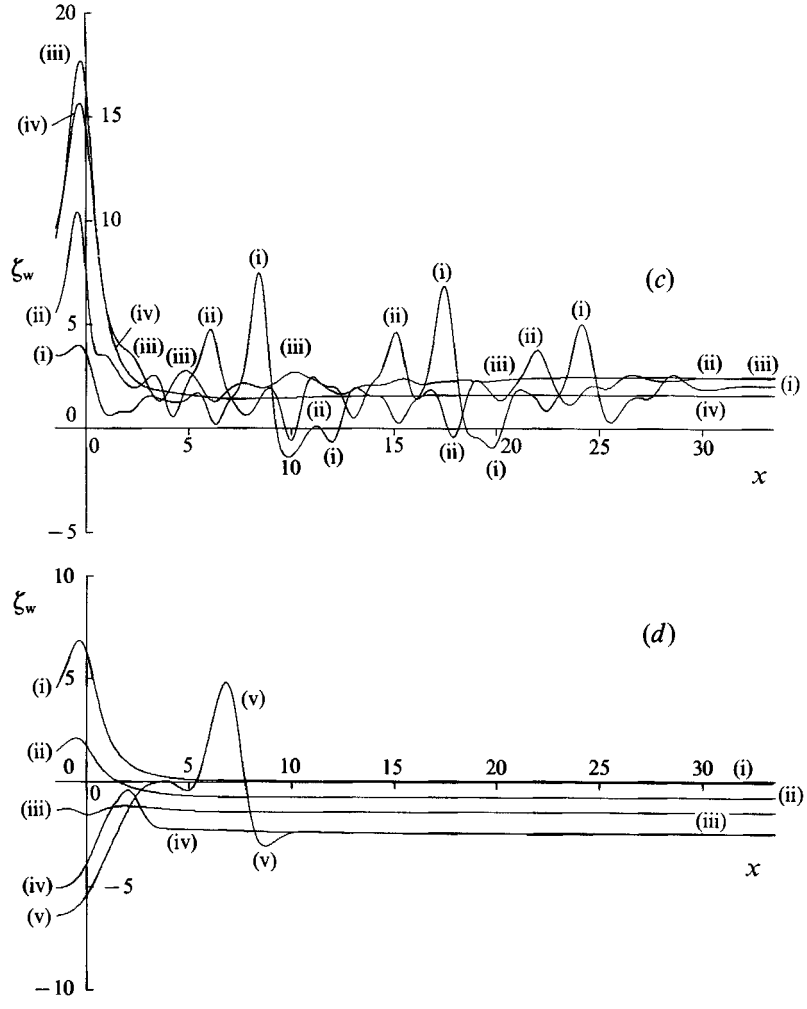

FIGURE 6. Lower-wall vorticity for figure 5: $Re = 500$, $St = 0.006$, $\epsilon = 1$. (*a*) $t = 0.05$, 0.10, 0.15, 0.20, 0.25 (i–v); (*b*) $t = 0.30$, 0.35, 0.40, 0.45, 0.50 (i—v); (*c*) $t = 0.55$, 0.60, 0.70, 0.80 (i–iv); (*d*) $t = 0.90$, 0.95, 1.00, 1.10, 1.20 (i–v).

The vorticity on the lower wall (shear stress) for this case is shown in figure 6. During the forward phase of the flow ($t < 0.5$; figure 6*a*, *b*) the lower-wall vorticity takes its peak positive values under the first eddies just upstream of the reattachment points, and its peak negative values just downstream of the reattachment points. As a result the shear gradient is very large near reattachment points. The regions with the lowest wall shear magnitude are at the upstream end of the eddies where the core flow has moved away from the wall (it is also of course small in the step corner as can be deduced from the streamline plots). These peak values of wall shear are much greater in magnitude than the values in the parallel flow far downstream. Note also that the peaks are not stationary but move with the (downstream end) of the eddies, and that they decrease in magnitude with successive eddies, reflecting the gradual downstream weakening of the wave.

When the flow reverses after $t = 0.5$, the peaks in the wall shear decay as the eddies are destroyed until by $t = 0.7$ (figure 6*c*) the residual waviness is relatively small with a large peak occurring near the step as the flow accelerates into the constricted part

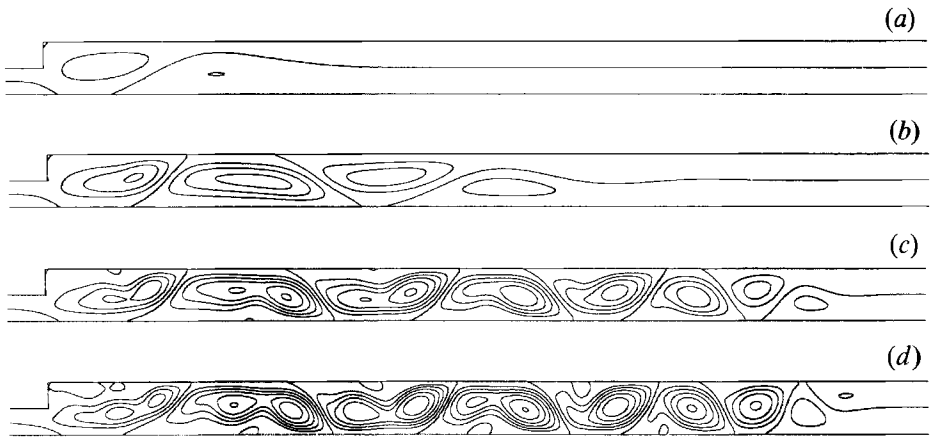

FIGURE 7. Effect of variation in the Reynolds number. Streamlines for $St = 0.006$, $e = 1$, $t = 0.5$, $-1.5 \leqslant x \leqslant 33.5$; (a) $Re = 125$, (b) $Re = 250$, (c) $Re = 500$, (d) $Re = 750$.

of the channel ($x < 0$). This peak decays in magnitude until at $t = 1.0$ (figure 6d) the vorticity on the lower wall shows relatively little variation. As the flow then accelerates down over the step at the start of the second cycle, the peak in vorticity downstream of the step is re-established. Note in particular the similarity between the vorticity at $t = 0.2$ (figure 6aiv) and $t = 1.2$ (figure 6dv).

4.2. *Variation of Reynolds number*

First, consider Reynolds numbers less than 500. In this range, decreasing Re decreases the amplitude of the wave, as can be seen in figure 7(a, b) which shows streamlines for $Re = 125$ and 250 at $t = 0.5$. Clearly the eddies are much weaker and have a simpler form than for $Re = 500$ (figure 7c). These plots suggest that with a lower Reynolds number the wave does not travel as far downstream as in the previous case. However, a detailed examination of the results for $Re = 250$ showed that a wave extends approximately as far downstream as for $Re = 500$, although it is much weaker. For $Re = 125$ there was also a wave much further downstream than is apparent from figure 7(a), although it could not be tracked as far downstream as for $Re = 250$ and 500.

The streamline pattern for $Re = 750$ at $t = 0.5$ is shown in figure 7(d). The wave here is basically similar to that shown in figure 7(c) for $Re = 500$, but, as might be expected, both the primary vortex wave and the secondary disturbance are stronger (see also table 1). In addition, both the total length of the wave and the (primary) wavelength are similar. This is further illustrated by figure 8 which shows the centre streamline for $Re = 250$, 500 and 750 with $St = 0.006$ and $\epsilon = 1$. Figure 8 also shows the initial downstream motion of the individual waves followed by a slight upstream motion before the flow reverses, as can be seen in figure 5 too, and demonstrates that the downstream peaks for $Re = 750$ are slightly further upstream than those for $Re = 500$. The latter result is consistent with a convected wavefront, as from $t = 0$ to 0.5 a particle in parallel flow will travel a distance of 34.8 when $Re = 750$ and 36.5 when $Re = 500$. As $Re \to \infty$ the unsteady flow in a parallel-sided channel tends to the potential solution of uniform flow in the channel, induced by vortex sheets at the walls. In this limit a particle travels a distance of $[\pi St(1+\epsilon)]^{-1}$, and this expression provides a lower bound for the distance a particle will travel in parallel flow (for $St = 0.006$ and $e = 1$ this value is 26.5 which is approached slowly as Re increases). An

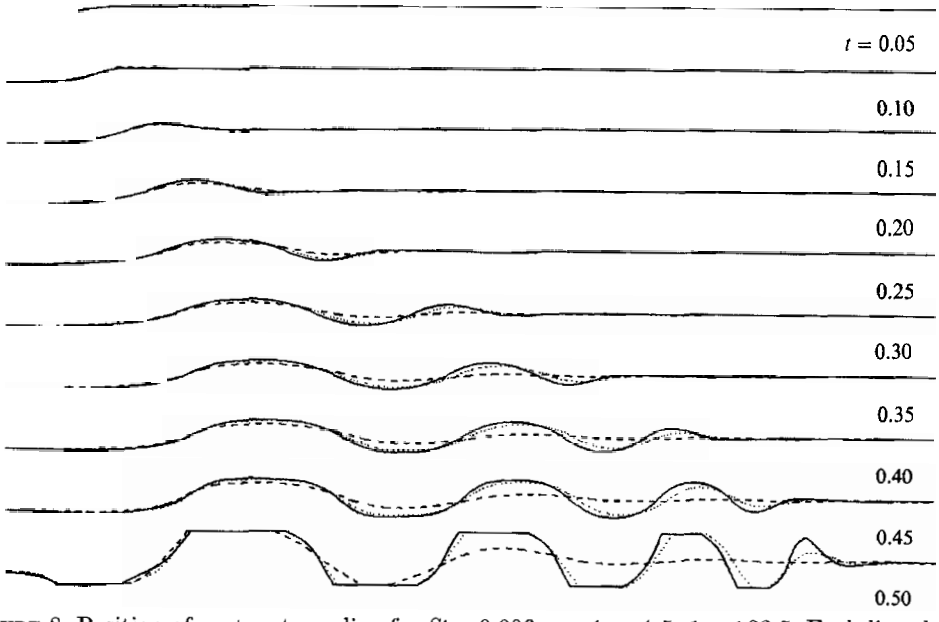

FIGURE 8. Position of centre streamline for $St = 0.006$, $\epsilon = 1$, $-1.5 \leqslant x \leqslant 33.5$. Each line shows the position of $\psi = \frac{1}{2}\psi_w$ (y against x). ---, $Re = 250$; ....., $Re = 500$; ——, $Re = 750$.

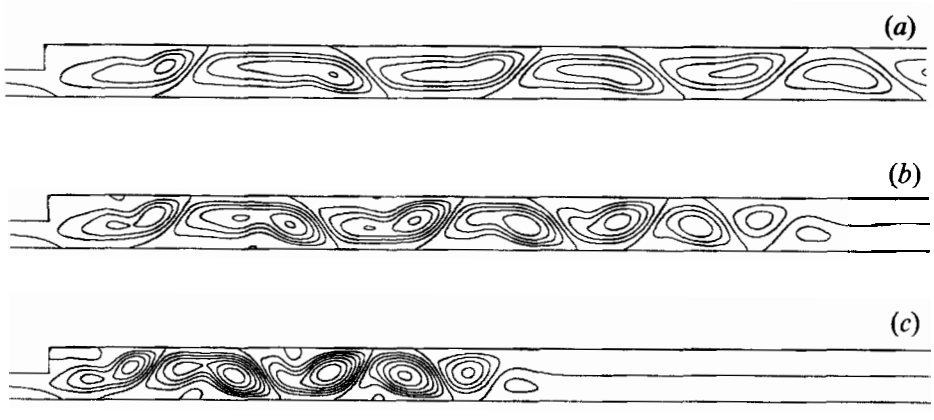

FIGURE 9. Effect of variation in the Strouhal number. Streamlines for $Re = 500$, $\epsilon = 1$, $t = 0.5$, $-1.5 \leqslant x \leqslant 33.5$: (*a*) $St = 0.004$, (*b*) $St = 0.006$, (*c*) $St = 0.010$.

upper bound for a particle in parallel flow, given by modulated Poiseuille flow, is 1.5 times the lower bound.

4.3. *Variation of Strouhal number*

If the wavefront is convected with the flow we would expect the total length of the wave to be (roughly) inversely proportional to the Strouhal number, as discussed above. Also, since an increase in St with no change in Re can be achieved by an increase in the frequency of the oscillation with no change in the peak mass flux, we might also expect a more vigorous response from the flow with an increase in strength of the vortex wave. Both of these predictions are borne out, as shown in figure 9 which displays the streamlines for $Re = 500$ at $t = 0.5$ with $St = 0.004$, 0.006, and 0.010. The increase in strength with St at other times can be seen from table 2. Clearly

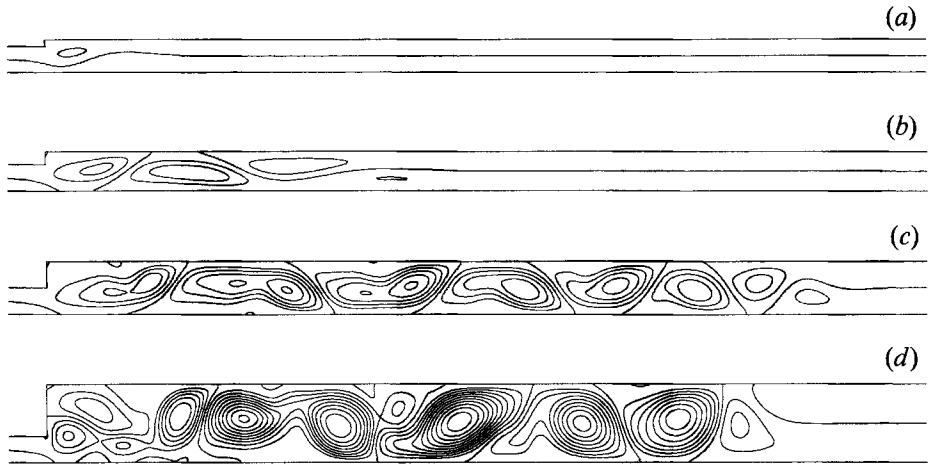

FIGURE 10. Effect of variation in the step size. Streamlines for $Re = 500$, $St = 0.006$, $t = 0.5$, $-1.5 \leqslant x \leqslant 33.5$: (a) $\epsilon = 0.25$, (b) $\epsilon = 0.5$, (c) $\epsilon = 1$, (d) $\epsilon = 2$.

$St =$	0.004		0.006		0.010	
t	l	u	l	u	l	u
0.05	0.000	0.014	0.000	0.008	0.000	0.003
0.10	0.000	0.063	0.000	0.073	0.000	0.063
0.15	−0.024	0.073	−0.010	0.087	0.000	0.114
0.20	−0.044	0.086	−0.057	0.095	−0.027	0.122
0.25	−0.056	0.098	−0.077	0.106	−0.101	0.127
0.30	−0.068	0.105	−0.092	0.117	−0.141	0.136
0.35	−0.083	0.109	−0.114	0.125	−0.169	0.148
0.40	−0.103	0.113	−0.143	0.135	−0.206	0.194
0.45	−0.138	0.127	−0.186	0.182	−0.258	0.257
0.50	−0.202	0.197	−0.255	0.258	−0.335	0.342

TABLE 2. Variation of maximum eddy strengths with the Strouhal number: l gives the minimum value of the streamfunction (which is zero on the lower wall) and u the difference between the maximum value of the streamfunction and the value on the upper wall. $Re = 500$, $\epsilon = 1$.

both the primary wave and the secondary disturbance increase in strength as St increases, while with Re and ϵ fixed the total length of the wave, the wavelength and the number of (primary) eddies generated increases when St decreases. Although the secondary disturbance is weaker, the eddies are still markedly asymmetric at the lowest Strouhal number considered here.

4.4. *Variation in step height* ϵ

Not surprisingly, one effect of decreasing the step size is to decrease the strength of the wave, as can be seen from figure 10 which shows the streamlines for $Re = 500$ and $St = 0.006$ at $t = 0.5$ with $\epsilon = 0.25$, 0.5, 1 and 2. In fact, for much of the time up to $t = 0.5$, the flow over a step of size 0.5 or less resembles steady flow over a backward-facing step (see e.g. Cherdron *et al.* 1978; Armaly *et al.* 1983; Durst & Pereira 1988) with a small number of relatively weak eddies showing back-to-front symmetry rather than the highly disturbed flow seen with a bigger step. However, even for a small step the eddies increase in size and strength with time, and the flow pattern is

$\epsilon =$	0.5		1		2	
t	l	u	l	u	l	u
0.05	0.000	0.005	0.000	0.008	0.000	0.007
0.10	0.000	0.016	0.000	0.073	0.000	0.134
0.15	0.000	0.019	−0.010	0.087	−0.010	0.274
0.20	0.000	0.023	−0.057	0.095	−0.178	0.296
0.25	0.000	0.026	−0.077	0.106	−0.308	0.312
0.30	−0.003	0.028	−0.092	0.117	−0.315	0.327
0.35	−0.011	0.031	−0.114	0.125	−0.317	0.365
0.40	−0.028	0.039	−0.143	0.135	−0.378	0.355
0.45	−0.063	0.060	−0.186	0.182	−0.368	0.433
0.50	−0.140	0.115	−0.255	0.258	−0.461	0.541

TABLE 3. Variation of maximum eddy strengths with the channel width: l gives the minimum value of the streamfunction (which is zero on the lower wall) and u the difference between the maximum value of the streamfunction and the value on the upper wall. $Re = 500$, $St = 0.006$.

not symmetric about $t = 0.25$, so cannot be said to be truly quasi-steady. Also, for $\epsilon = 0.25$ and 0.5 the wave could not be tracked as far downstream as a particle travels in parallel flow.

The effect on the flow of varying Re and St was investigated for $\epsilon = 0.5$. The changes were qualitatively similar to those described above for $\epsilon = 1$: i.e. the wavelength and total length of the wave are only weakly dependent on Re but inversely proportional to St, and the strength of both the primary wave and secondary disturbances increase as Re or St is increased. There is one important difference, however, in that even for the strongest waves, the total wave is much shorter than the distance travelled by a particle in parallel flow: for $St = 0.006$ the wavefront reaches $x = 30$ (approximately) whereas a particle in parallel flow would travel to $x = 48.0$ by $t = 0.5$. Thus a mechanism based on a wavefront simply convected by the parallel flow ahead of the wave cannot be invoked to explain the generation of the wave in this channel.

The flow in channels with $\epsilon > 1$ was also investigated. For $Re = 500$ and $St = 0.006$ the total length of the wave was shorter but stronger for $\epsilon = 2$ than for $\epsilon = 1$ (see figure 10*d*). As ϵ was increased further, up to 4, the wave increased in strength and slowly decreased in length. A comparison with the distance travelled by a particle in parallel flow, which is almost inversely proportional to the channel width when Re and St are held constant, showed that, in contrast to the case with $\epsilon < 1$, the parallel-flow calculation underestimates the length of the wave for $\epsilon > 1$, the difference increasing with ϵ. However, a change in Re and St has the same general effect as before.

For the range of parameters considered here, our calculations showed that with Re and St held constant, the (primary) wavelength increases as ϵ increases, provided the wave is fully established (this is opposite to the predictions of the simple model of Tutty & Pedley 1992). Also, the wave increases in strength as the step size increases, as can be seen from table 3 which gives the maximum eddy strengths for $\epsilon = 0.5$, 1, and 2 with $Re = 500$ and $St = 0.006$ (note that the erratic changes in the values given for $\epsilon = 2$ are due to a change in the relative strength of different eddies rather than a sudden change in the flow).

We have used the minimum (left) channel width as the lengthscale for non-dimensionalization. Instead, we could have used the maximum (right) width and

varied the step size by varying the width on the left. This would be most easily accomplished by geometrically rescaling the present problem and expressing the results in terms of the Strouhal number $St_r = (1+\epsilon)^2 St$ (the Reynolds number is independent of the channel width and therefore is not affected by the rescaling). Comparing (the rescaled) results for $\epsilon = 0.5$, 1, and 2 with $St_r = 0.024$ (i.e. $St = 0.006$ when $\epsilon = 1$), we found that, again, increasing the step size (i.e. decreasing the width on the left) leads to a stronger wave with a longer (primary) wavelength. Also, as implied by the above discussion comparing the motion of the wavefront with that of a particle in parallel flow, the total length of the wave increases as the step size is increased while the other parameters are held constant.

5. Generation and development of the vortex wave

As an alternative to the simple convective model, which is not fully consistent with the numerical results, we will now consider, in turn, the generation and development of both the primary wave and the secondary disturbance in terms of vortex dynamics.†

The streamlines and vorticity distribution for $Re = 500$, $St = 0.006$, and $\epsilon = 2$ are shown in figure 11 (plates 1 and 2). We see that, as the flow is accelerated from rest, vorticity generated on the upper wall upstream of the step is swept into the channel from the corner, forming a tongue of vorticity which then rolls up. The vorticity convected back towards the step forms the core of the main eddy which develops in the lee of the step. The positive vorticity in this eddy will act to pull the core flow immediately downstream of the eddy towards the upper wall, and thus enhance the natural motion of the fluid away from the lower wall as the core flow expands to fill the channel; by $t = 0.15$ negative vorticity generated at the lower wall is being convected away from the wall to form another tongue. Overlaying streamlines and velocity vectors on the vorticity distribution showed that the vorticity is carried away from the lower wall by the core flow, rather than being ejected by a local process of breakaway separation. In turn, the second tongue of vorticity rolls up to form the core of the first major eddy on the lower wall, which grows in strength and size as the rollup continues, with the core flow displaced towards the upper wall. By $t = 0.2$ a region of negative vorticity exists in the centre of the channel, forming a 'vortex' which acts to pull the flow immediately downstream of the eddy away from the upper wall and thereby help to create another tongue of (positive) vorticity which is convected away from the wall and in turn rolls up to form the core of the next eddy on the upper wall. This process continues with eddies being created successively on the upper and lower walls. Note that the characteristic 'backward sloping' shape which the eddies take as they develop is a natural consequence of their formation by the rollup of a tongue of vorticity (see e.g. $t = 0.25$ in figure 11), and that, with the possible exception of the eddy formed in the lee of the step, the rollup of the tongues of vorticity is not in this problem initiated by entrainment of the vorticity into existing eddies; rather vorticity rolls up to form the initial major core in each flow structure.

† The description of the wave development expounded here is based on a detailed examination of the solutions for a large number of cases. The behaviour of the flow was studied by overlaying streamlines and/or velocity vectors on colour-coded vorticity plots, including cases where the local dynamical behaviour was examined by calculating the velocity relative to the movement of the eddies. Of necessity, only a few of these plots can be reproduced here; these were selected to illustrate as clearly as possible the important stages in the development of the flow.

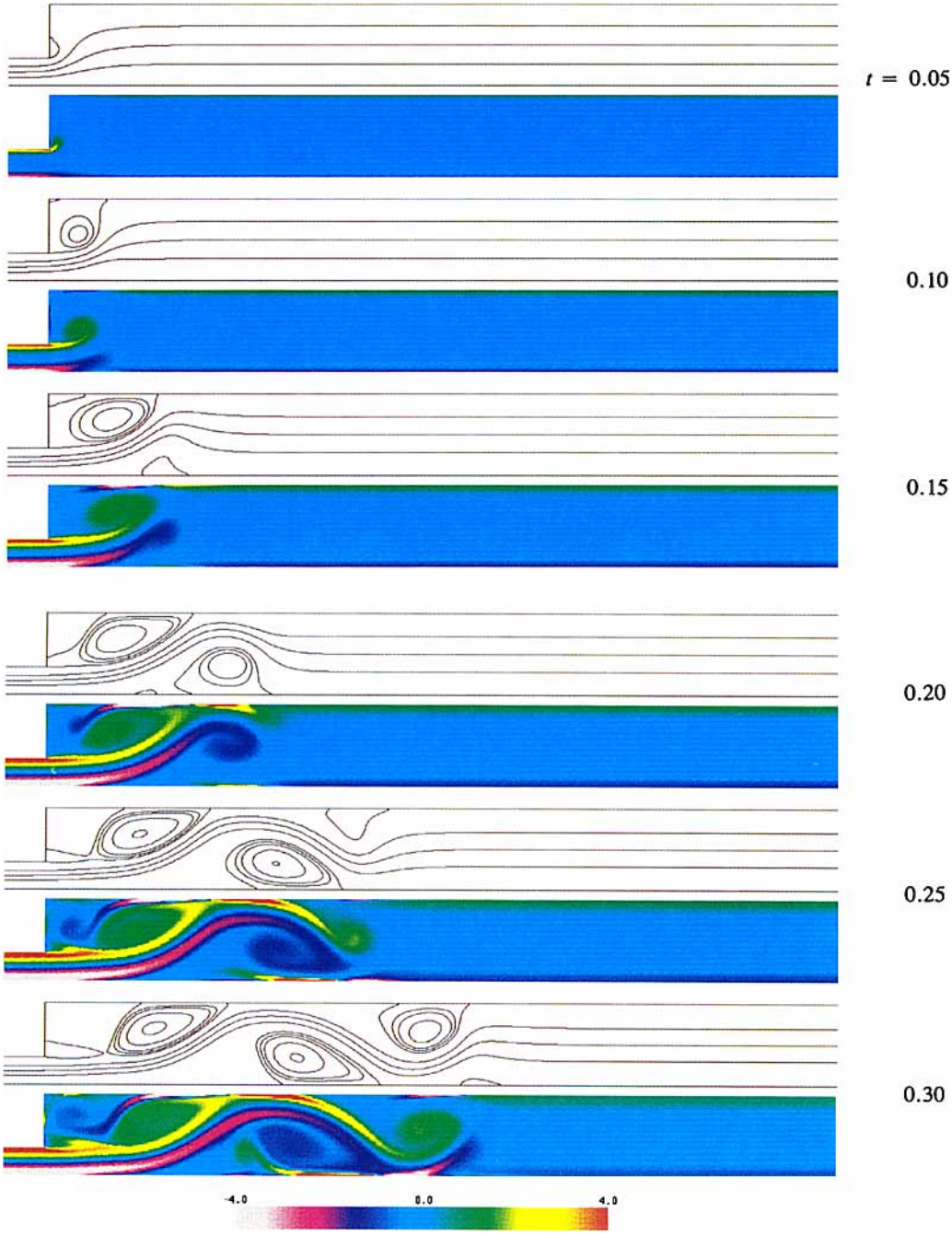

FIGURE 11. For caption see next page.

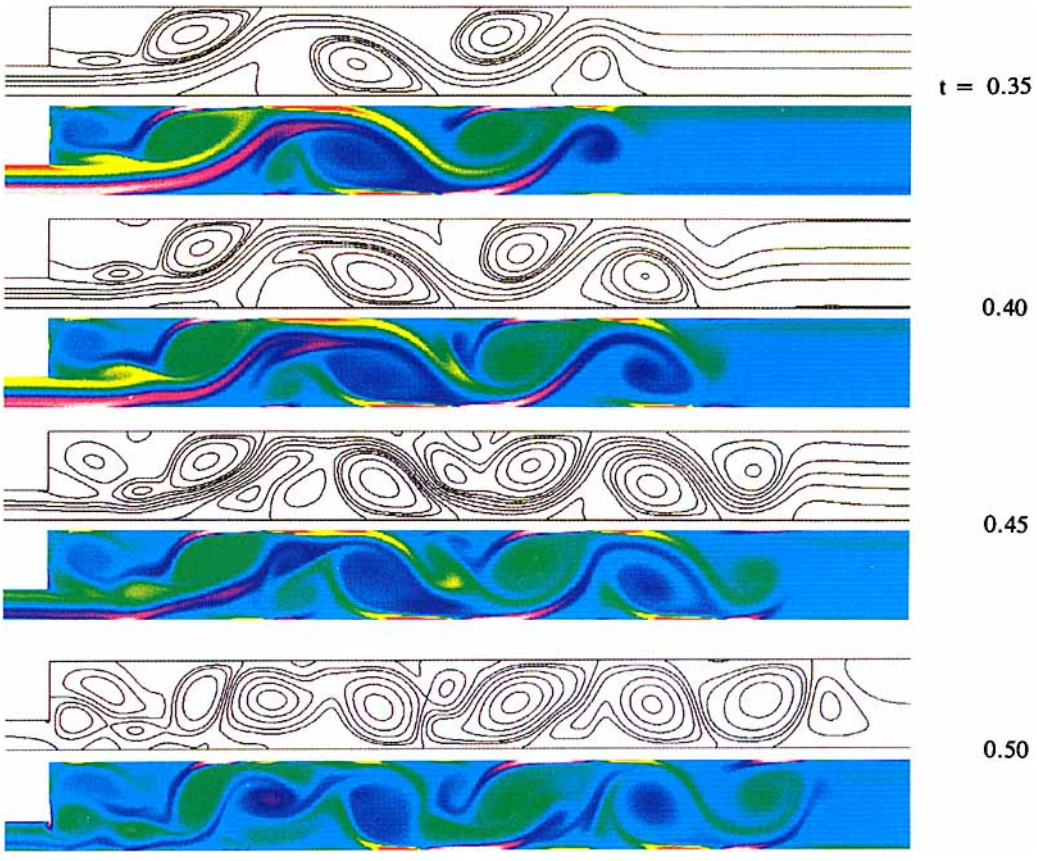

FIGURE 11. Streamlines and vorticity for $Re = 500$, $St = 0.006$, $\varepsilon = 2$, $-1.5 \leq x \leq 29$: $t = 0.05$ to 0.5 in steps of 0.05. The streamfunction is plotted for $\psi = -0.05, 0.05$ and in increments of 0.1 above ψ_w and below zero, and in increments of ¼ ψ_w between zero and ψ_w.

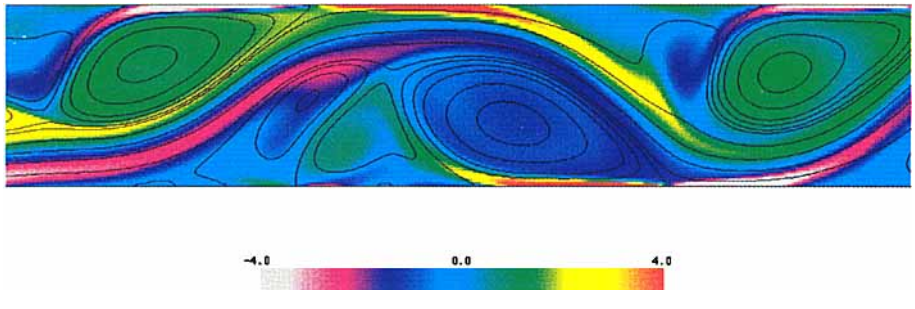

FIGURE 12. Streamlines and vorticity for $Re = 500$, $St = 0.006$, $\varepsilon = 2$, $t = 0.375$, $2.5 \leq x \leq 17.5$. Same streamfunction values as for figure 11.

Turning to the secondary disturbance, we will now argue that this can also be explained in terms of vortex dynamics. Considering the first major eddy/flow structure formed on the lower wall, we see that, as the negative vorticity convected from the wall into the centre of the channel rolls up to form the characteristic backward sloping eddy, which is evident by $t = 0.25$, positive vorticity is generated at the wall by the reverse flow in the eddy near the wall. This vorticity is convected away from the wall into a region with relatively low velocity, where by $t = 0.3$ the tongue has rolled up and there is a 'comma' shaped region of positive vorticity between the wall and the core flow immediately upstream of the main eddy; the head of the 'comma' forms the core of a positively rotating eddy (marked as B1 on figure 13*a* below). Simple vortex dynamics suggest that the presence of this 'vortex' close to the core flow will result in a local deceleration of the core flow, and indeed by $t = 0.3$ there is an appreciable thickening of the core shear layer in this region (figure 11). By $t = 0.35$ negative vorticity originally carried by the core flow has been convected away by the action of the positive vortex (B1) to create a narrow tongue of negative vorticity extending from the core flow towards the wall (figure 11), which by $t = 0.375$ (figure 12, plate 2) forms the core of an elongated eddy upstream of the primary eddy (C1 on figure 13*b*). The two (negative) eddies (A1 and C1 on figure 13*b*) join by $t = 0.4$, with the tongue of vorticity that was convected from the core lying along the arm of the primary eddy which extends to the upstream wall.

By $t = 0.425$, a small negative eddy (D1, figure 13*d*) has formed between the core flow and the positive eddy B1, with its vorticity coming from the region of concentrated negative vorticity lying at the top of the arm of A1 at $t = 0.4$. The original core (A1) continues to grow in strength. By $t = 0.45$ eddy D1 forms one of two co-rotating cores of a much larger eddy, with flow which previously went below eddy B1 changing direction and now going below the second core (E1, figure 13*e*). Also, there is a noticeable thickening of the core shear layer with a concentration of negative vorticity on the left of E1, caused it appears by a change in the path of the core flow at about $t = 0.425$, and, possibly, diffusion of vorticity from the high-vorticity, high-velocity core flow to the low-vorticity, low-velocity region near the wall. This vorticity rolls up and feeds into eddy E1, which grows rapidly until by $t = 0.475$ D1 has vanished as a separate core, with its vorticity for the most part being entrained into E1. By $t = 0.5$, E1 is slightly stronger than A1, while B1 has been destroyed with its vorticity convected along the lower side of E1. Similarly, positive vorticity has been convected from eddy A0 along the top side of E1 (figure 11).

Examining the flow in the lee of the step we see a similar pattern, but with a different final structure due to the presence of the step. Downstream, however, each major eddy structure develops in the same manner, but at any given time they are at different stages of development as they have existed for successively shorter times. For example, at $t = 0.45$ the second structure on the lower wall is similar to, but shorter than, the first at $t = 0.35$. Note, however, that unlike B1, eddy B2 (figure 13) is not destroyed, and that although it is very weak by $t = 0.45$ it then grows again as it is fed negative vorticity, mainly from that generated by A2 at the wall, but with a contribution from the vorticity generated on the upper wall by the mainstream.

In general, we have found that the wavelength decreases with distance along the channel, which is consistent with a convective mechanism as the later eddies are generated when the flow is decelerating, and thus the vorticity would not be carried as far downstream. Also, the later eddies will be weaker as they have less time to develop. After they are formed the eddies/wave crests move downstream for a time, but start moving back towards the step before the mass flow reverses at $t = 0.5$ (see

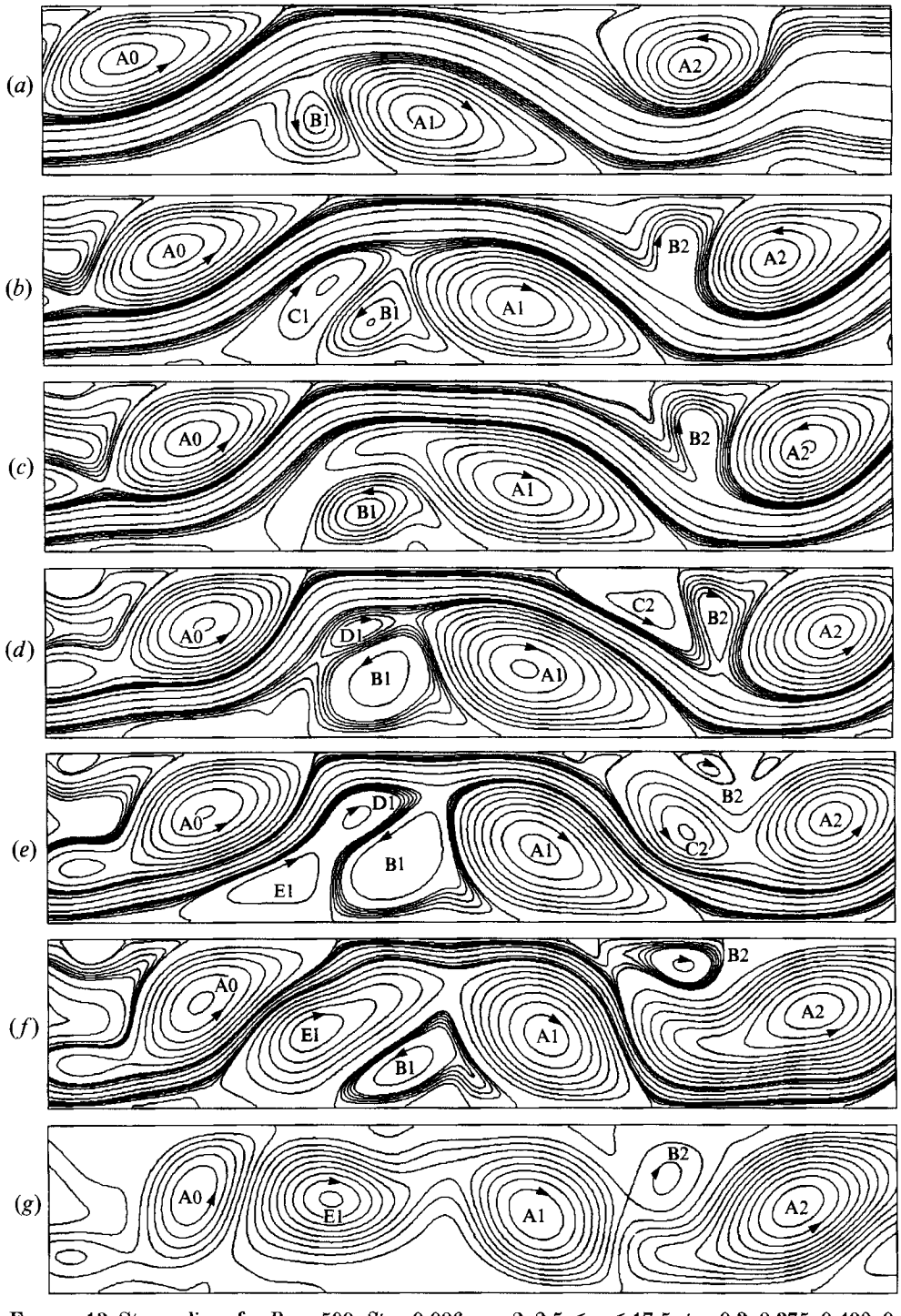

FIGURE 13. Streamlines for $Re = 500$, $St = 0.006$, $\epsilon = 2$, $2.5 \leqslant x \leqslant 17.5$: $t = 0.3, 0.375, 0.400, 0.425, 0.45, 0.475, 0.5$ (*a–g*). Usual values (i.e. as for figure 5) with extra values close to zero (positive) and ψ_w (less than ψ_w) in (*a–f*).

e.g. figure 8). This phenomenon can be interpreted in terms of vortex dynamics by considering the inviscid flow in a channel given by a system of image vortices, as suggested by Ralph & Pedley (1989), where the vortices would translate towards the step unless there was counterbalancing advection, e.g. by the mainstream.

It remains to consider the effects of parameter variation. The cross-sectionally averaged dimensionless velocity is inversely proportional to the Strouhal number but independent of the Reynolds number, and since the proposed mechanism relies on vorticity convected away from the walls by the core flow, we might expect that the total length of the wave will obey the same relationship. For a given ϵ this criterion was found to give a reasonable estimate provided Re was large enough. For lower Re (e.g. $Re = 250$ with $\epsilon = 1$; figure 7*b*) the tongues of vorticity convected away from the wall were both thicker and weaker, and, not surprisingly, were much less inclined to roll up and form the strong, asymmetric, eddies found at higher Re.

In §4 we found that the distance travelled by a particle at the centre of the channel in parallel flow gave a reasonable estimate of the total length of the wave for $\epsilon = 1$, but overestimated the length of the wave with a smaller step and underestimated it for a larger step. A detailed examination of the solution for $\epsilon = 0.5$, $Re = 2000$, and $St = 0.006$, showed that, while the development of the wave was broadly similar to that described above for $\epsilon = 2$, the displacement of the streamlines away from the wall and the rollup of vorticity were restricted by the reduced width of the channel, and that the streamwise velocity of the fluid carrying the vorticity away from the wall is significantly less than the centreline velocity in parallel flow. In contrast, for $\epsilon = 2$, the core flow between the eddies occupies a relatively narrow region of the channel, and near the wavefront the fluid carrying the vorticity away from the walls has a streamwise velocity that is consistently significantly greater than the corresponding centreline velocity for parallel flow. Thus vorticity is convected downstream at a rate greater than that predicted by parallel flow. Hence, again, the results are consistent with the mechanism proposed above.

The wavelength (i.e. the length of an individual flow structure) increases with the step size. This can be explained by observing that with a larger step the vorticity is convected further away from the walls and thus has more space and time to roll up before reattaching to the wall at the downstream end of the eddy, which also explains why there are fewer eddies/flow structures with a larger step. That, for a given step size, the wavelength decreases as the Strouhal number increases (figure 9) is consistent with fluid particles travelling a distance inversely related to the Strouhal number.

6. Further discussion

The present results may be compared with the experimental observations by Sobey (1985) of flow in a three-dimensional rectangular channel with aspect ratio 7.5:1. The experiments covered a smaller range of Re than our calculations, and for a right-angled asymmetric expansion were restricted to $\epsilon = 1$. Sobey found instabilities and three-dimensional effects at higher Reynolds numbers that are absent from the above predictions, so only a limited comparison can be made. However, there is good qualitative agreement, particularly with respect to the generation of a vortex wave, the general shape and motion of the eddies, and the effect of varying the Strouhal number. In addition to the experiments, Sobey performed a small number of calculations for flow in a periodic channel using a different finite difference method to that used here. Although Sobey's calculations

were for a somewhat different geometry, there is general consistency between his results and ours.

We can also compare our results with those from related problems. Tutty (1992) gave numerical results for pulsatile flow (with a non-zero mean mass flux) in a locally constricted channel. A vortex wave was found with essentially the same behaviour and parameter dependence as described above. Pedley & Stephanoff (1985) and Ralph & Pedley (1988, 1989, 1990) studied the flow in a channel where a disturbance is imposed on an otherwise steady flow by a sinusoidal oscillation of a portion of one wall. Although the mainstream did not reverse in that problem, the experiments and calculations showed the generation of a vortex wave which in many ways is similar to that shown in figure 5 above. There are however some notable differences. For example, the eddies propagate downstream, albeit with a phase velocity which was lower than the wavefront velocity by a factor of 2.3 to 4.6.

Further, our results do not show 'eddy doubling', the asymmetric evolution of an eddy which initially shows a significant degree of fore-aft symmetry, with the closed streamlines concentrating near the reattachment point and the eddy eventually splitting into two, as found in the moving-wall problem. Examining the results of Ralph & Pedley (1988), in particular figure 4, we see that it is only the two eddies closest to the indentation that split, and that the eddies further downstream have the characteristic backward-sloping appearance found above. Ralph & Pedley identified the process of eddy doubling with the convection of vorticity towards the downstream end of the eddy, resulting in an increasing degree of non-symmetry, and the generation of vorticity of the opposite sign on the wall and its subsequent convection around the eddy and into the channel. Clearly, this process is consistent with the mechanism for wave generation presented in §5 above, the difference being that the wave/eddy already existed in the moving-wall case before vorticity generation at the wall and vortex dynamics came into play, whereas in the present case it is the vortex dynamics that generate the eddies. As the strength of the wave increases in the moving-wall problem, so does the similarity with our results (see figure 10 of Ralph & Pedley 1988).

For the moving-wall problem, the inviscid, long-wavelength, small-amplitude theory of Pedley & Stephanoff (1985) predicted the formation of a wavetrain during each cycle. In that theory the displacement of the core-flow streamlines satisfies a linearized Korteweg–de Vries equation. Predictions of wave crest positions were compared with experimental results and with values from Navier–Stokes and Euler calculations (Pedley & Stephanoff 1985; Ralph & Pedley 1988, 1989, 1990), with reasonable agreement. In particular, the results from the Euler solution for a small-amplitude wall disturbance and the inviscid theory agreed almost perfectly as long as account was taken of the acceleration and deceleration of the downstream mean flow caused by the motion of the indentation.

A similar inviscid, small-amplitude theory can be derived for flow in a rigid non-uniform channel with an unsteady mean flow (Tutty & Pedley 1992). The theory assumes a small-amplitude perturbation to a non-reversing parallel flow in a channel with a smooth change in width, not oscillatory flow in a stepped channel. However, in the moving-wall case the correct pattern of behaviour was predicted in regions of parameter space which, strictly, are outside the range of validity of the theory, and a qualitative comparison can be made for the present problem. For flow into an expansion, Tutty & Pedley (1992) predict the existence of a wave with positive group and zero phase velocity, i.e. a standing wave with a wavefront propagating downstream, and a wavelength that is only weakly dependent on Re, which agrees

with our results. However, in the theory the wave is generated during acceleration of the flow, and the wavelength is (essentially) independent of St, which does not agree. In addition, the theory predicts that the wavelength will decrease as the step height increases, whereas our numerical results show the reverse trend. For flow into a constriction, Tutty & Pedley (1992) predict at best a very weak wave, which agrees with the present results. We note that solutions for pulsatile flow (i.e. with a non-zero mean) in a constricted channel (Tutty 1992), which might be expected to show a better agreement with the theory, showed a pattern of behaviour similar to that found here, and thus also disagrees with the theory in important respects.

The computations of Ralph & Pedley (1989), in which the Euler equations were solved for the moving-wall problem with rotational, Poiseuille flow upstream, showed that the primary wave generation process is essentially inviscid in that problem, involving only the redistribution of the upstream vorticity. Comparison with the Navier–Stokes calculations for the same problem, however, demonstrated that the secondary disturbance and eddy doubling require the presence of viscosity. We could compute an inviscid rotational flow in our channel, but it would in one important sense be arbitrary in that there is no natural rotational flow to impose upstream. In fact the inviscid limit for the present problem is the time-modulated potential flow with the streamlines given by the grid lines Y = constant (see figure 2).

Both our results and those of the moving-wall problem suggest that for a vortex wave to form the combination of geometry and flow conditions must be such that concentrated regions of (relatively) strong vorticity can form in the channel. In our problem, vorticity is shed naturally from the step into the expansion during forward flow, but not during reverse flow; some vorticity is shed similarly from the indentation in the viscous moving-wall problem, but there is also a mechanism for vorticity concentration that is essentially inviscid: as shown in the inviscid computation of Ralph & Pedley (1989), the motion of the indentation, and the consequent movement of the streamlines away from the wall, allows the formation of an eddy in the lee of the indentation consisting of fluid which was originally near the wall and thereby carrying strong vorticity. In contrast, with the grooved channel of Ghaddar *et al.* (1968*a*, *b*), shear layers form across the mouths of the grooves but this vorticity is not carried into the channel, and although relatively large-scale unsteady effects were found, these did not take the form of a vortex wave, at least for the range of parameters considered by Ghaddar *et al.*, even when the flow was subjected to an oscillatory perturbation at the resonant frequency (Ghaddar *et al.* 1986*b*).

Neither the primary vortex wave nor the secondary disturbance have been examined in terms of a standard unforced flow instability, e.g. in terms of Tollmien–Schlichting or Rayleigh waves, as the predictability and robustness of the phenomena reported here suggests that a more deterministic approach is appropriate, unlike, for example, some of the results reported by Ralph & Pedley (1990) for a channel with a moving indentation.

One motivation for this work comes from the conjectured relationship between regions of low and oscillating wall shear stress (vorticity) and the pattern of development of atherosclerosis in mammalian arterial blood vessels. Being two-dimensional the problem is highly idealized from a physiological viewpoint, but the results suggest that, even for a relatively low-frequency unsteady flow, an expansion in the vessel will lead to a complex pattern of wall shear stress with peak values far in excess of those found in a uniform vessel, while a flow into a constriction will be much simpler. Further, the distribution of regions of the vessel walls subject to

consistently higher or lower than average shear stress will depend in a non-trivial manner on the flow parameters and the geometry. The only constant prediction is that the wall shear stress in the immediate lee of the step/expansion will be low.

This work was supported by the UK Science and Engineering Research Council.

REFERENCES

ARMALY, B. F., DURST, F., PEREIRA, J. C. F. & SCHONUNG, B. 1983 Experimental and theoretical investigation of backward-facing step flow. *J. Fluid Mech.* **127**, 473–496.

CHERDRON, W., DURST, F. & WHITELAW, J. H. 1978 Asymmetric flows and instabilities in symmetric ducts with sudden expansions. *J. Fluid Mech.* **84**, 13–31.

DENNIS, S. C. R. & HUDSON, J. D. 1989 Compact explicit h^4 finite-difference approximations to operators of Navier–Stokes type. *J. Comput. Phys.* **85**, 390–416.

DURST, F. & PEREIRA, J. C. F. 1988 Time-dependent laminar backward-facing step flow in a two-dimensional duct. *Trans. ASME* I: *J. Fluids Engng* **110**, 289–296.

GHADDAR, N. K., KORCZAK, K. Z., MIKIC, B. B. & PATERA, A. T. 1986*a* Numerical investigation of incompressible flow in grooved channels. Part 1. Stability and self-sustained oscillations. *J. Fluid Mech.* **163**, 99–127.

GHADDAR, N. K., MAGEN, M., MIKIC, B. B. & PATERA, A. T. 1986*b* Numerical investigation of incompressible flow in grooved channels. Part 2. Resonance and oscillatory heat-transfer enhancement. *J. Fluid Mech.* **168**, 541–567.

KU, D. N., GIDDENS, D. P., ZARINS, C. K. & GLAGOV, S. 1985*a* Pulsatile flow and atherosclerosis in the human carotid bifurcation: positive correlation between plaque location and low and oscillating shear stress. *Arteriosclerosis* **5**, 293–302.

KU, D. N., PHILLIPS, D. J., GIDDENS, D. P. & STRANDNESS, D. E. 1985*b* Hemodynamics of the normal human carotid bifurcation: in vitro and in vivo studies. *Ultrasound Med. Biol.* **11**, 13–26.

PEDLEY, T. J. & STEPHANOFF, K. D. 1985 Flow along a channel with a time-dependent indentation in one wall: the generation of vorticity waves. *J. Fluid Mech.* **160**, 337–367.

RALPH, M. E. & PEDLEY, J. T. 1988 Flow in a channel with a moving indentation. *J. Fluid Mech.* **190**, 87–112.

RALPH, M. E. & PEDLEY, T. J. 1989 Viscous and inviscid flows in a channel with a moving indentation. *J. Fluid Mech.* **209**, 543–566.

RALPH, M. E. & PEDLEY, T. J. 1990 Flow in a channel with a time dependent indentation in one wall. *Trans. ASME* I: *J. Fluids Engng* **112**, 468–475.

SOBEY, I. J. 1985 Observation of waves during oscillatory channel flow. *J. Fluid Mech.* **151**, 395 426.

SRIDHAR, K. P. & DAVIS, R. T. 1985 A Schwarz–Christoffel method for generating two-dimensional flow grids. *Trans. ASME* I: *J. Fluids Engng* **107**, 330–337.

TUTTY, O. R. 1992 Pulsatile flow in a constricted channel. *J. Biomech. Engng* **114**, 50–54.

TUTTY, O. R. & PEDLEY, T. J. 1992 Unsteady flow in a non-uniform channel: a model for wave generation. (In preparation.)

WOODS, L. C. 1954 *Aeronaut. Q.* **5**, 176.